Supplementary information

Figure S1

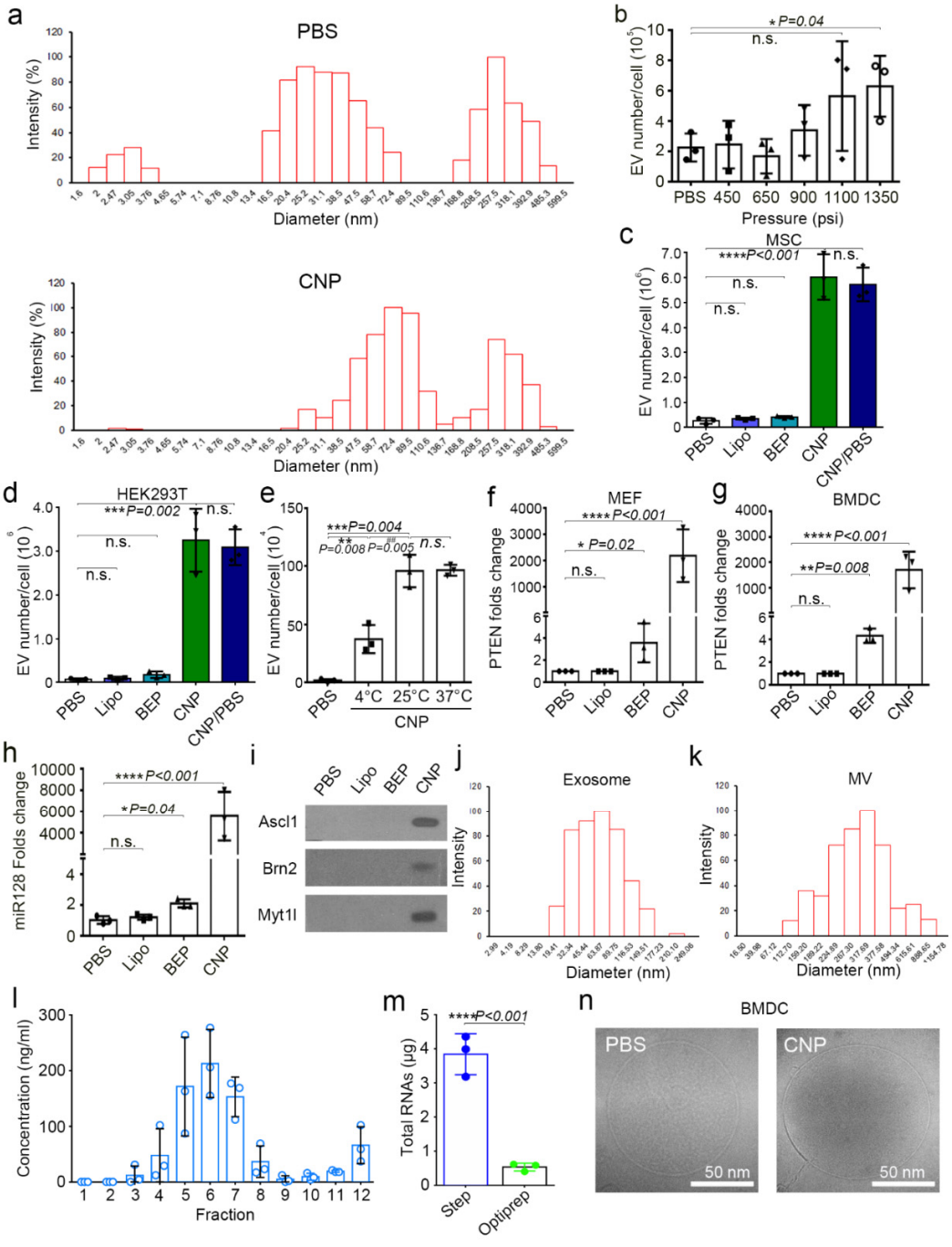

Figure S1. Characterization of exosomes generated from CNP. a. DLS measurement of vesicle size distribution produced by CNP. A peak around 70~110 nm was observed in the CNP group, suggesting the massive production of exosomes by CNP treatment. upper: PBS group, below: CNP group. **b.** DLS measurements of exosome number per cell in MEFs by gene gun at various pressures. Results show that the EV number increases slightly with the increase of pressure used in gene gun. Data are from three independent experiments and are presented as mean ± s.e.m. *P< 0.05, vs. PBS, Student t-test. **c.** EV number per cell

produced by mouse mesenchymal stem cells (MSCs) in different treatment groups, including PBS, Lipo, BEP, CNP, and CNP/PBS groups. **d.** EV number per cell produced by human embryonic kidney 293T (HEK293T) in different treatment groups, including PBS, Lipo, BEP, CNP, and CNP/PBS groups. **e.** EV number per cell produced by MEFs in CNP group at different temperatures of CNP operation. **f.** qPCR measurements of *PTEN* mRNA in EVs produced by various transfection methods with PTEN plasmid show that EVs produced by CNP contain much higher quantities of transcribed *PTEN* mRNAs than other methods in MEFs. **g.** qPCR measurements of *PTEN* mRNA in EVs produced by various transfection methods with PTEN plasmid show that EVs produced by CNP contain much higher quantities of transcribed PTEN mRNAs than other methods in BMDCs. **h**. qPCR measurements of miR-128 levels in EVs produced by various transfection methods with miR-128 plasmid show that EVs produced by CNP contain much larger quantities of transcribed miR-128 than other methods in MEFs. **i.** Western blot of *in vitro* protein translation in total vesicles secreted from MEFs by different transfection methods, suggesting that the total vesicles containing transcribed mRNA are able to translate into functional protein. **j.** DLS measurement of vesicle size distribution produced by CNP in the exosome fraction collected by ultracentrifugation. **k.** DLS measurement of vesicle size distribution produced by CNP in the microvesicle (MV) fraction collected by ultracentrifugation. **l.** RNA amount in each fraction from 10^8 CNP-transfected MEFs isolated by Optiprep™ gradient ultracentrifugation. The majority of RNAs are within the exosome-rich fractions (Fraction 5-7). **m.** RNA amount in exosomes from 10^8 CNP-transfected MEFs measured by Nanodrop. Multi-step ultracentrifugation (Step) has higher RNA recovery efficiency than Optiprep™ gradient ultracentrifugation (Optiprep). **P< 0.01, vs Step. **n.** Cryo-TEM images showed similar appearances of exosomes (BMDC) from PBS and CNP group (CNP). All data are from three independent experiments unless otherwise stated and are presented as mean ± s.e.m. Two-sided Student's t-test was performed for the comparison (**b, c, d, e, f, g, h, m**).

Figure S2

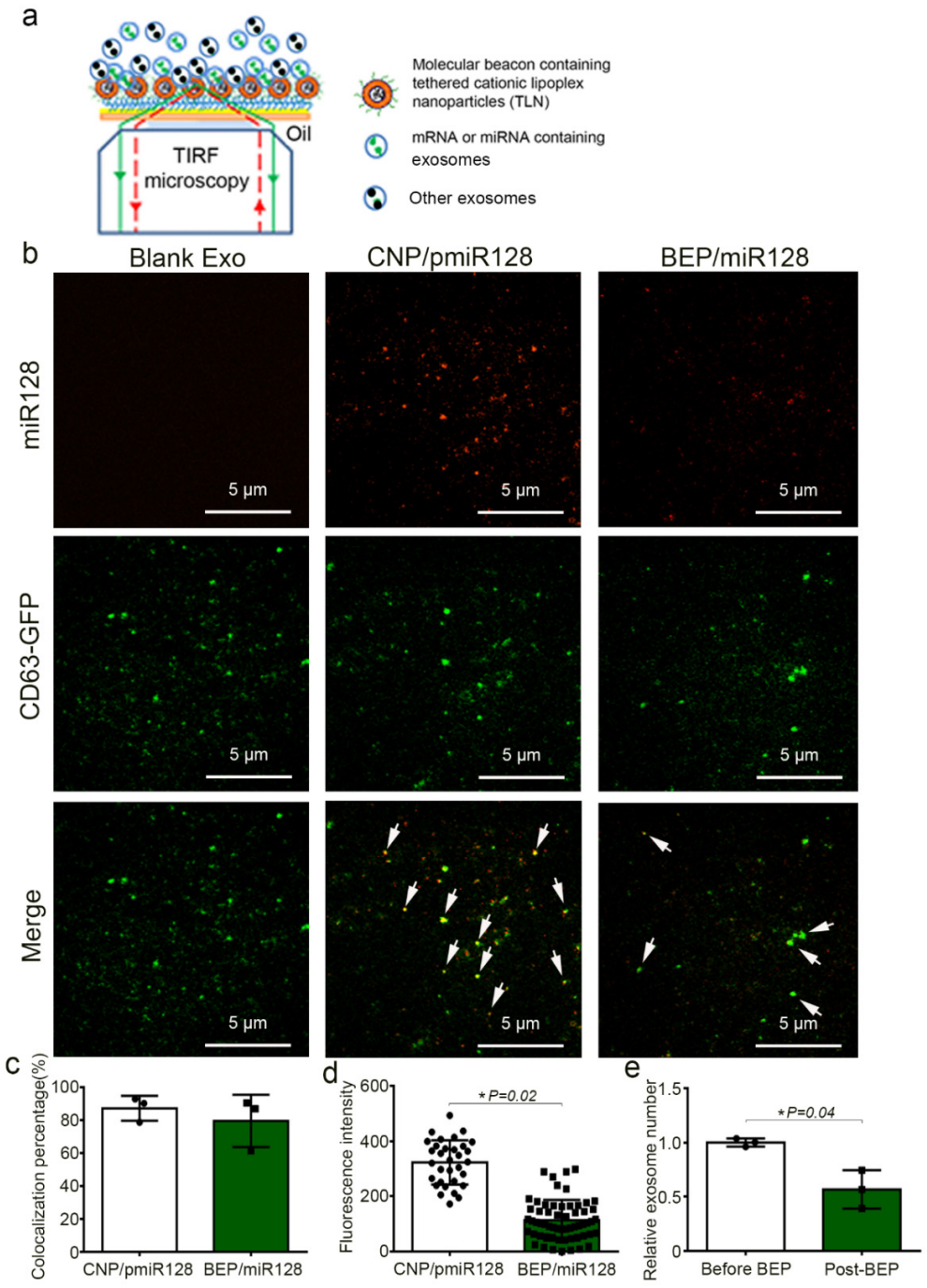

Figure S2. Comparison of CNP with BEP on miRNA loading efficiency into exosomes. a. Schematic demonstration of the procedure for tethered lipoplex nanoparticle (TLN) assay. Nanoparticles containing specific molecular beacon (MB) are tethered onto a glass coverslip, and exosomes are captured by nanoparticles. Hybridization of mRNA inside exosomes with the MB inside the nanoparticles produces fluorescence, which is detected by total internal refractory microscopy (TIRF). **b.** Representative TIRF images of TLN assay of miR-128 colocalized in exosomes (CD63-GFP) after CNP and BEP show that CNP has a better miRNA-128-loading

efficiency into exosomes compared to BEP. **c.** Colocalization percentage of miR-128 in exosomes after CNP and BEP. 100 images are used for statistical analysis. **d.** miR-128 fluorescence intensity within exosomes measured by TLN in CNP and BEP groups. 100 images are used for statistical analysis. **e.** DLS measurements of relative exosome numbers before and after BEP show that BEP breaks around 50% of exosomes. Data are from three independent experiments unless otherwise stated and are presented as mean ± s.e.m. Two-sided Student's t-test was performed for the comparison (**c, d, e**).

Figure S3

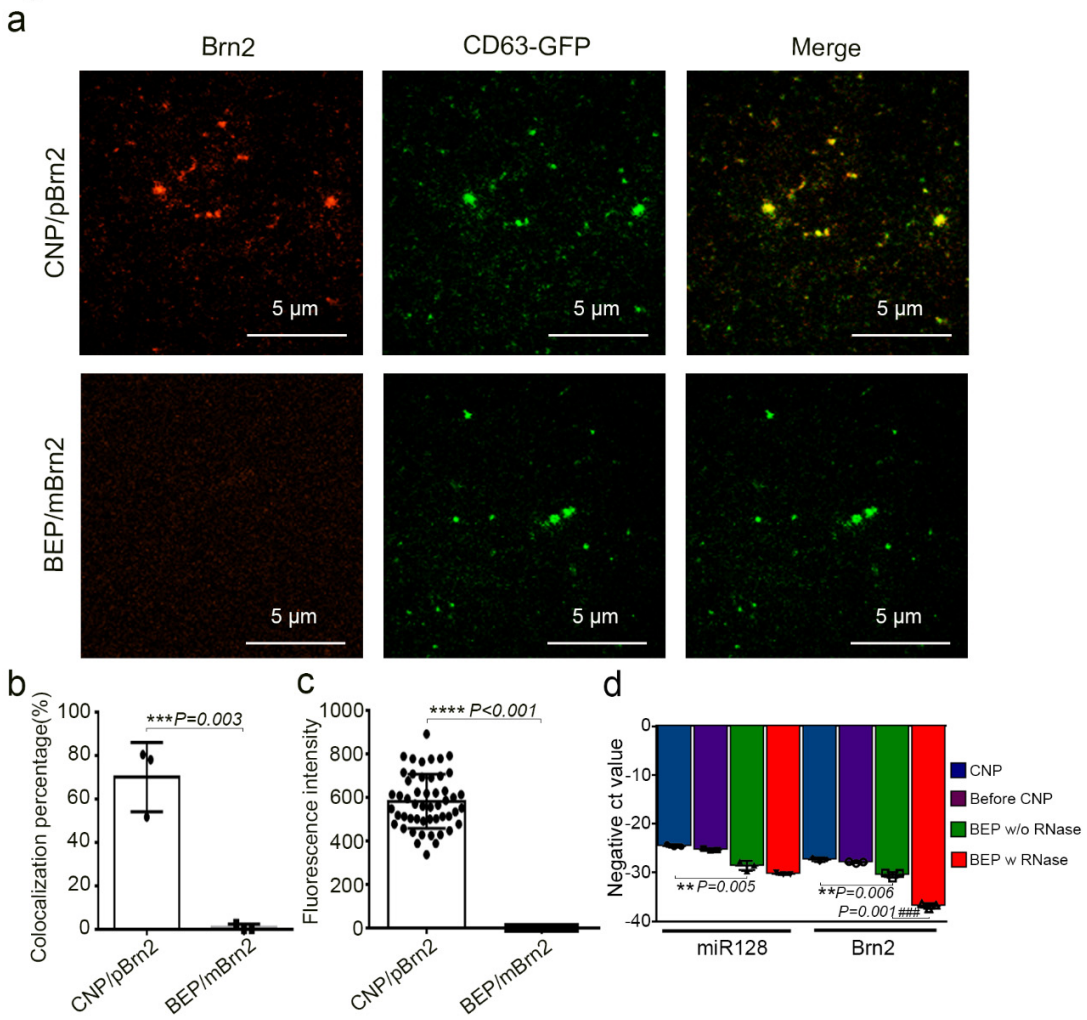

Figure S3. Comparison of CNP with BEP on mRNA loading efficiency into exosomes. a. Representative images of TLN assay of *Brn2* mRNA colocalized in exosomes (CD63-GFP) after CNP and BEP show that CNP has a much higher mRNA loading efficiency into exosomes than BEP. **b.** Colocalization percentage of *Brn2* mRNA in exosomes after CNP and BEP. 100 images are used for statistical analysis. **c.** *Brn2* mRNA fluorescence intensity within EVs as measured by TLN in CNP and BEP groups. 100 images are used for statistical analysis. **d.** qPCR of miR-128 and *Brn2* mRNA expression (CT value) of exosomes secreted from 10^7 CNP-transfected MEFs (CNP), free RNA from 10^7 CNP-transfected MEFs mixed with exosomes from 10^7 CNP/PBS transfected MEFs (Mixture), exosomes from Mixture after bulk electroporation-based RNA insertion (BEP w/o RNase), and RNase treated exosomes from Mixture after BEP to remove RNA molecules attached on exosome outer surface (BEP w RNase). All data are from three independent experiments unless otherwise stated and are presented as mean ± s.e.m. Two-sided Student's t-test was performed for the comparison (**b, c, d**).

Figure S4

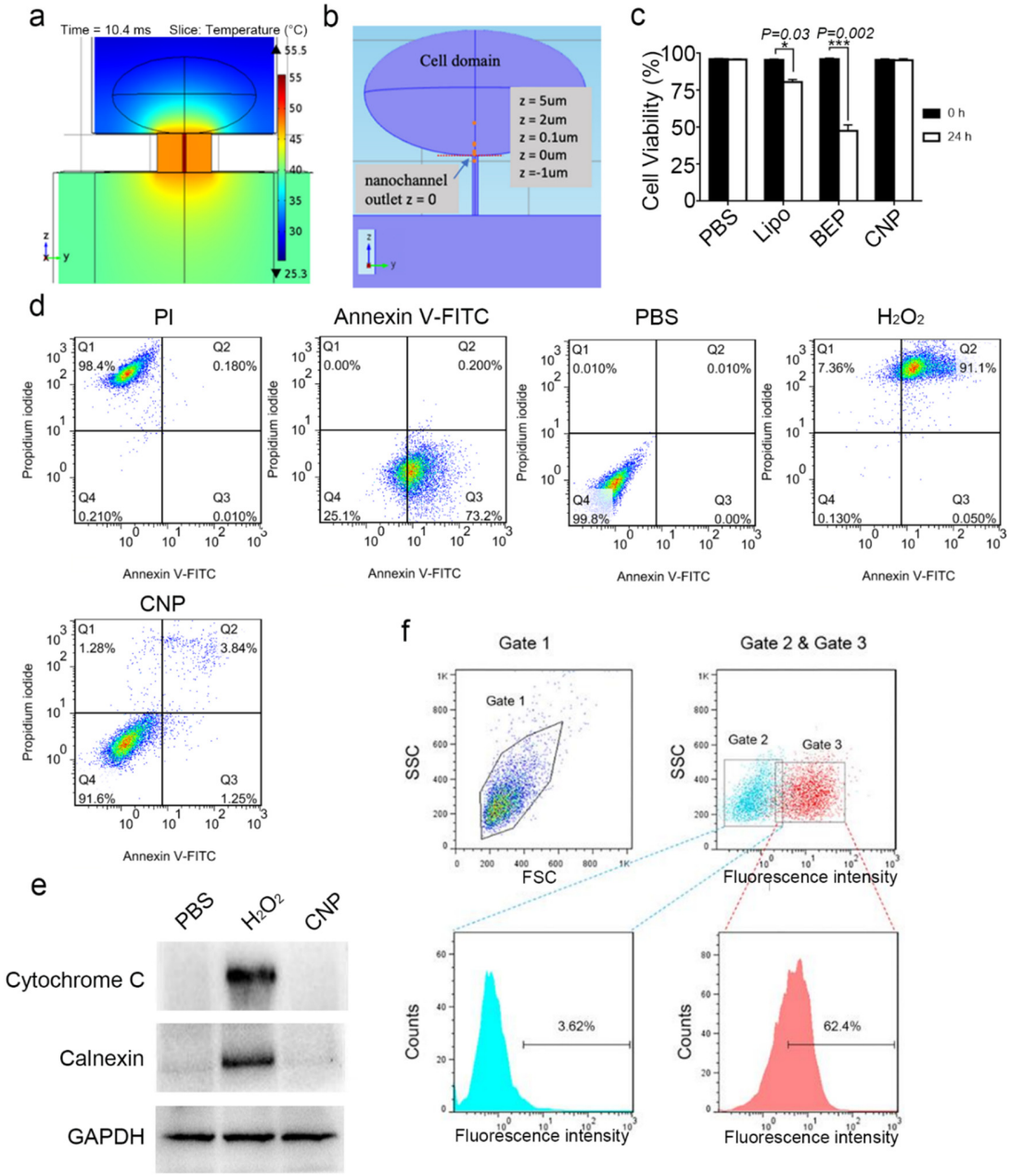

Figure S4. Cell death and apoptosis after CNP. a. Schematic demonstration of temperature rise in a single nanochannel. **b.** Selected 5 different locations in/near nanochannel. **c.** MTS cell viability assay with different treatments at different time points shows that CNP did not induce significant amounts of cell death. All data are from three independent experiments and are presented as mean ± s.e.m. Two-sided Student t-test was performed for the comparison**. d.** Flow cytometry analyses of annexin V and PI stains reveals no significant upregulation in cell apoptosis following CNP. H_2O_2 was used as a positive control for apoptosis. **e.** Western blot of the cell lysis after CNP treatment shows no elevation in apoptotic body markers as compared to PBS control group, while the H_2O_2 positive control group showed significant increases in these apoptotic proteins. **f.** Gating thresholds for the analysis of exosomes by flow cytometry.

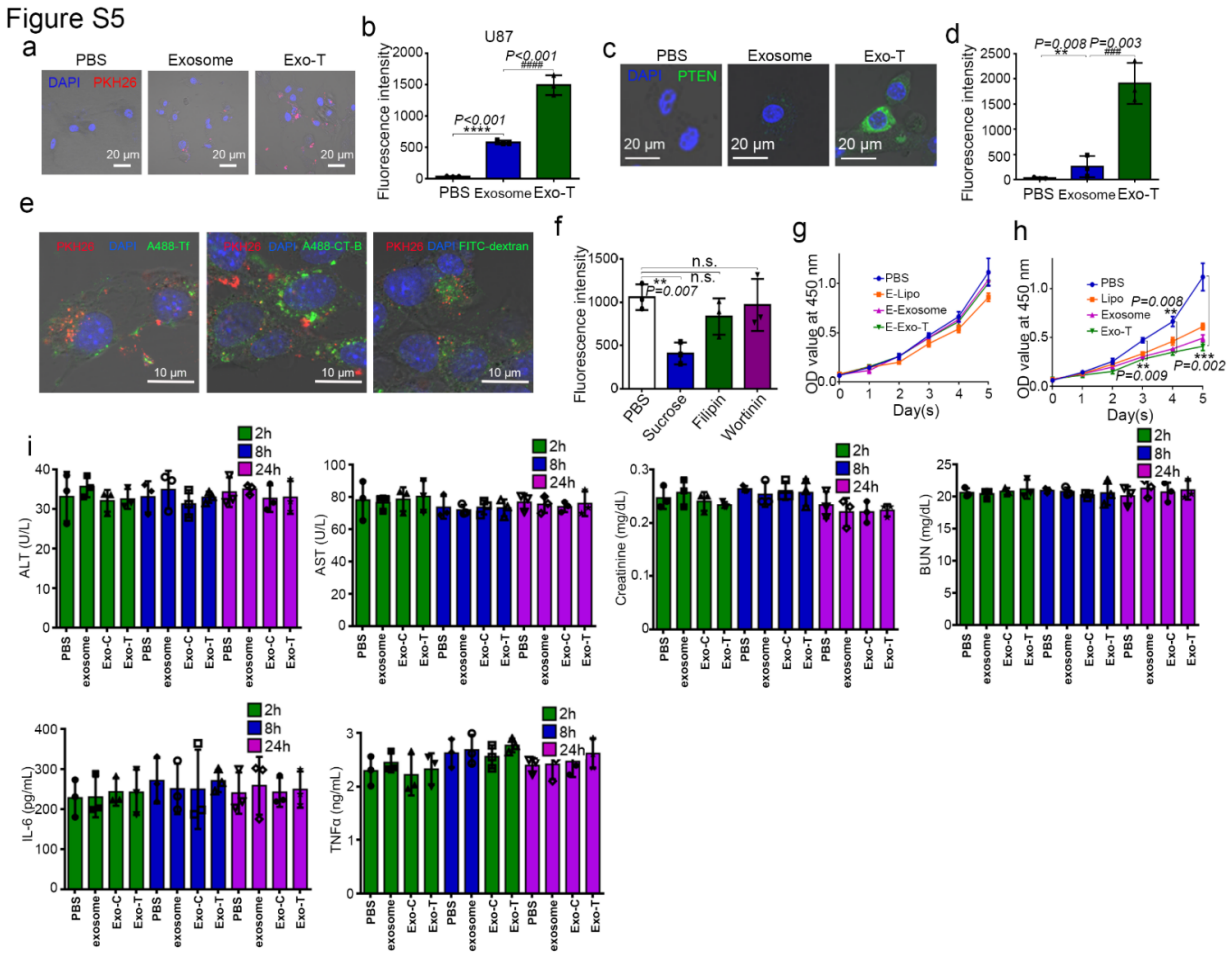

Figure S5. ***In vitro*** **study of CNP generated exosomes for gene therapy in U87 cells. a.** Increased uptake of CNP-generated exosomes coated with a brain tumour targeting peptide (CDX) linked to CD47 by glioma (U87) cells. Exosome: uncoated exosomes. Exo-T: exosomes generated from CNP stimulated MEFs transfected with CDX-CD47 plasmid. **b**. Fluorescence intensity of PKH26-labeled Exo-T taken up by U87 by flow cytometry further confirms Exo-T has the better uptake in U87 cells. **c.** Representative confocal microscopy images of PTEN staining in U87 cells 24 h after PBS, exosome or Exo-T treatments. **d**. Fluorescence intensity of PTEN staining 24 h after incubation of U87 with exosomes by flow cytometry shows the Exo-T group has stronger PTEN protein expression. **e.** Representative immunostaining images of co-localization of PKH26-labeled Exo-T vesicles (red) with different endocytosis markers (green). Results indicate the majority of Exo-Ts are co-localized with A488-Tf, suggesting Exo-Ts are mainly taken up through clathrin-dependent endocytosis. A488-Tf: Clathrin-dependent endocytosis marker; A488-CT-B: Caveolae-dependent endocytosis marker; and FITC-dextran: Macropinocytosis marker. **f.** Fluorescence intensity of PKH26-labeled Exo-T taken up by U87 under different inhibition conditions by flow cytometry further confirms Exo-Ts are mainly taken up through clathrin-dependent endocytosis. Sucrose: Clathrin-dependent endocytosis inhibitor; Filipin: Caveolae-dependent endocytosis inhibitor, and Wortinin: Macropinocytosis inhibitor. **g.** U87 cell viability treated by empty lipofectamine (E-Lipo), exosome and Exo-T suggests good biocompatibility of Exo-T. **h.** U87 cell viability treated by lipofectamine, exosome and Exo-T containing PTEN mRNA. **i.** AST, ALT, creatinine, BUN, IL6 and TNFα levels measured by ELISA at various time points in mice with different types of exosomes. Results show that Exo-T has no obvious *in vivo* toxicity or immunogenicity in mice. All data are from three independent experiments unless otherwise stated and are presented as mean ± s.e.m. Two-sided Student's t-test was performed for the comparison**.** (**b, d, f, g, h, i**).

Figure S6

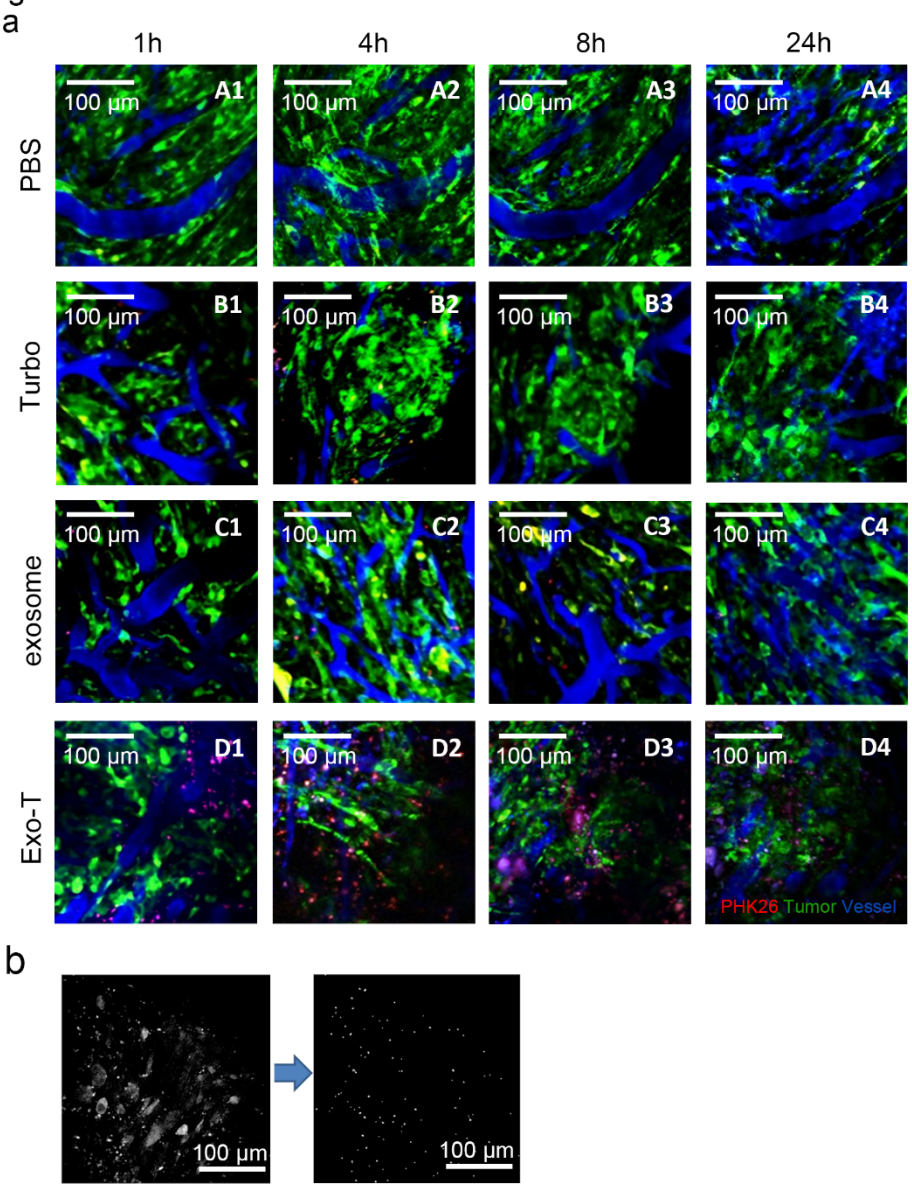

Figure S6. ***in vivo*** **biodistribution of Exo-Ts within the tumor interstitium**. **a**. Representative intravital fluorescence images in mouse GBM tumor stroma at various time points post administration of different nanocarriers labeled with PKH26 show that Exo-T has a better GBM tumor accumulation compared to other treatments. n=3 mice for each group. Four-hour images were also present in Figure 8b. **b**. Segmentation of exosomes conjugated with PKH26 from the whole image.

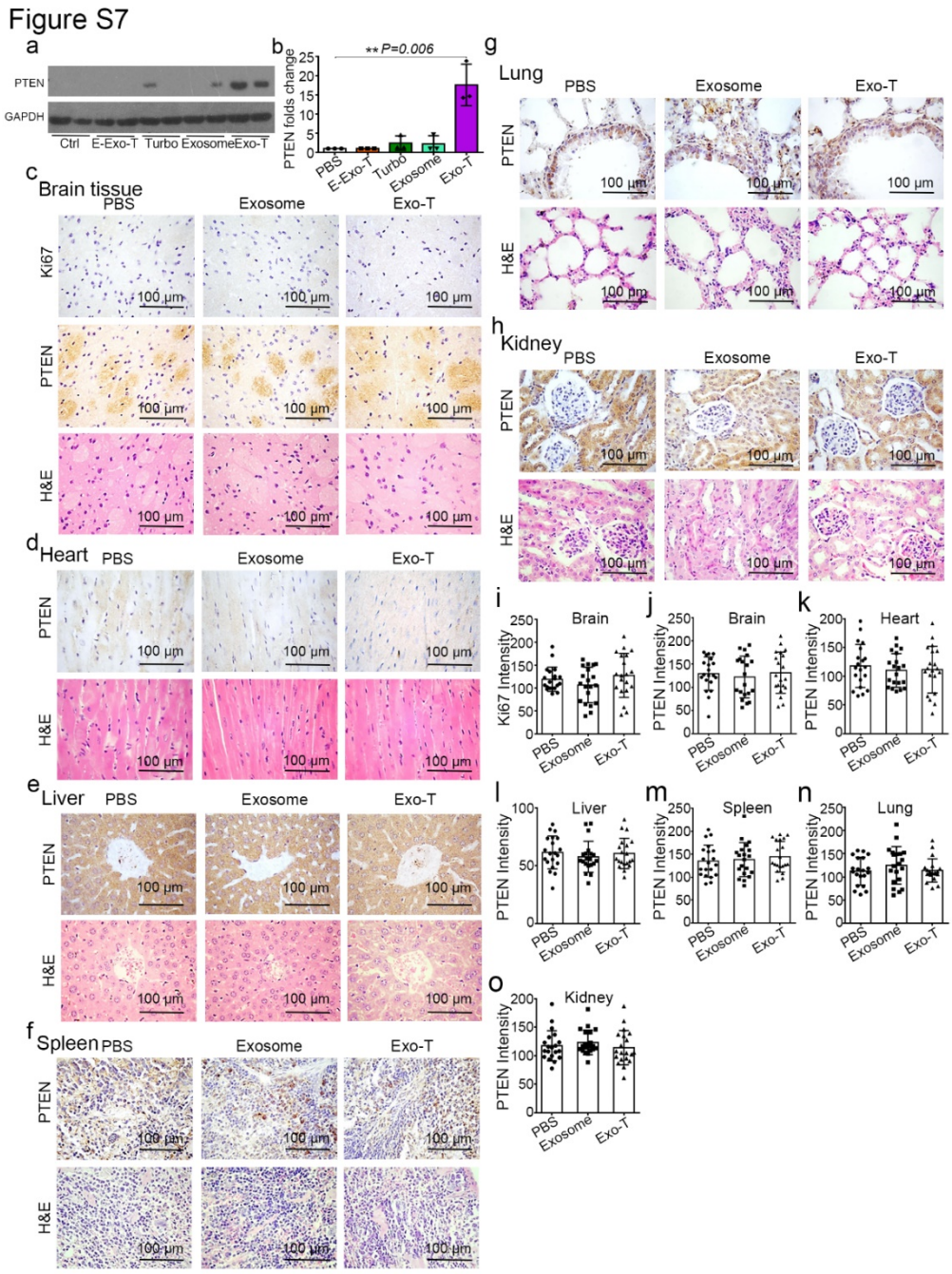

Figure S7. Immunohistochemistry staining of different tissues in a U87 orthotopic glioma model. a, b. Western blots (**a**) and qPCR (**b**) of PTEN protein and mRNA levels respectively in GBM tumours, suggest the restoration of both PTEN protein and mRNA expression in *PTEN*-null U87 GBM tumour. n=3 mice per group. **c,** PTEN, Ki67 and H&E staining of normal brain tissue with different treatments shows no direct effect on normal brain tissue. **d-o.** PTEN and H&E staining of heart, liver, spleen, lung and kidney tissue with different treatments show that Exo-T exhibits no detectable effect on the tissues examined. Magnification: x400. All data are from twenty independent images and are presented as mean ± s.e.m. Two-sided Student's t-test was performed for the comparison (i-o)**.**

Figure S8

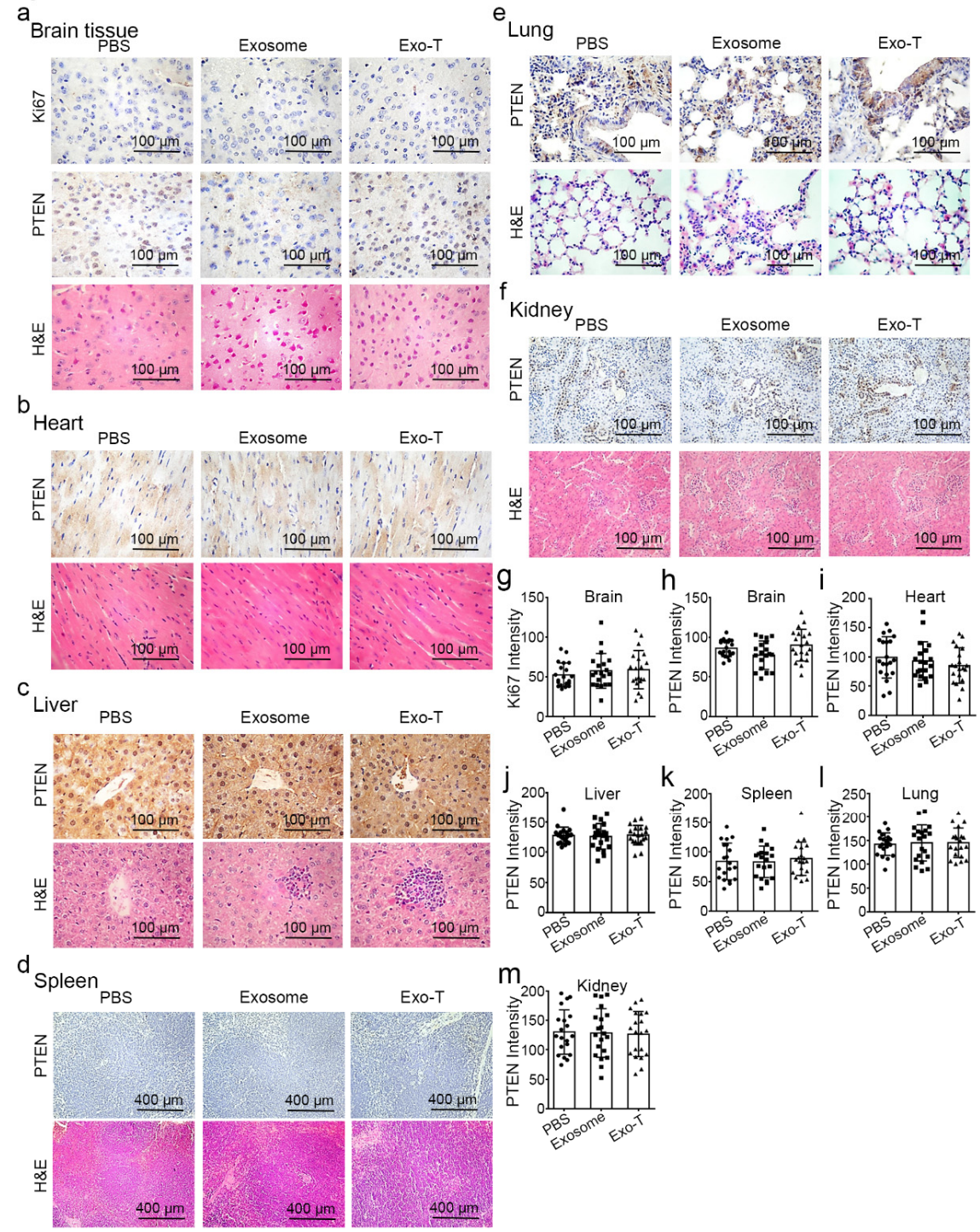

Figure S8. Immunohistochemistry staining of different tissues in a GL261 orthotopic glioma model. a, PTEN, Ki67 and H&E staining of normal brain tissue with different treatments shows no direct effect on normal brain tissue. **b-f.** PTEN and H&E staining of heart, liver, spleen, lung and kidney tissue with different treatments show that Exo-T exhibits no detectable effect on the tissues examined. Magnification: x400. Spleen: 100X. All data are from twenty independent images and are presented as mean ± s.e.m. Two-sided Student's t-test was performed for the comparison (g-m).

Figure S9

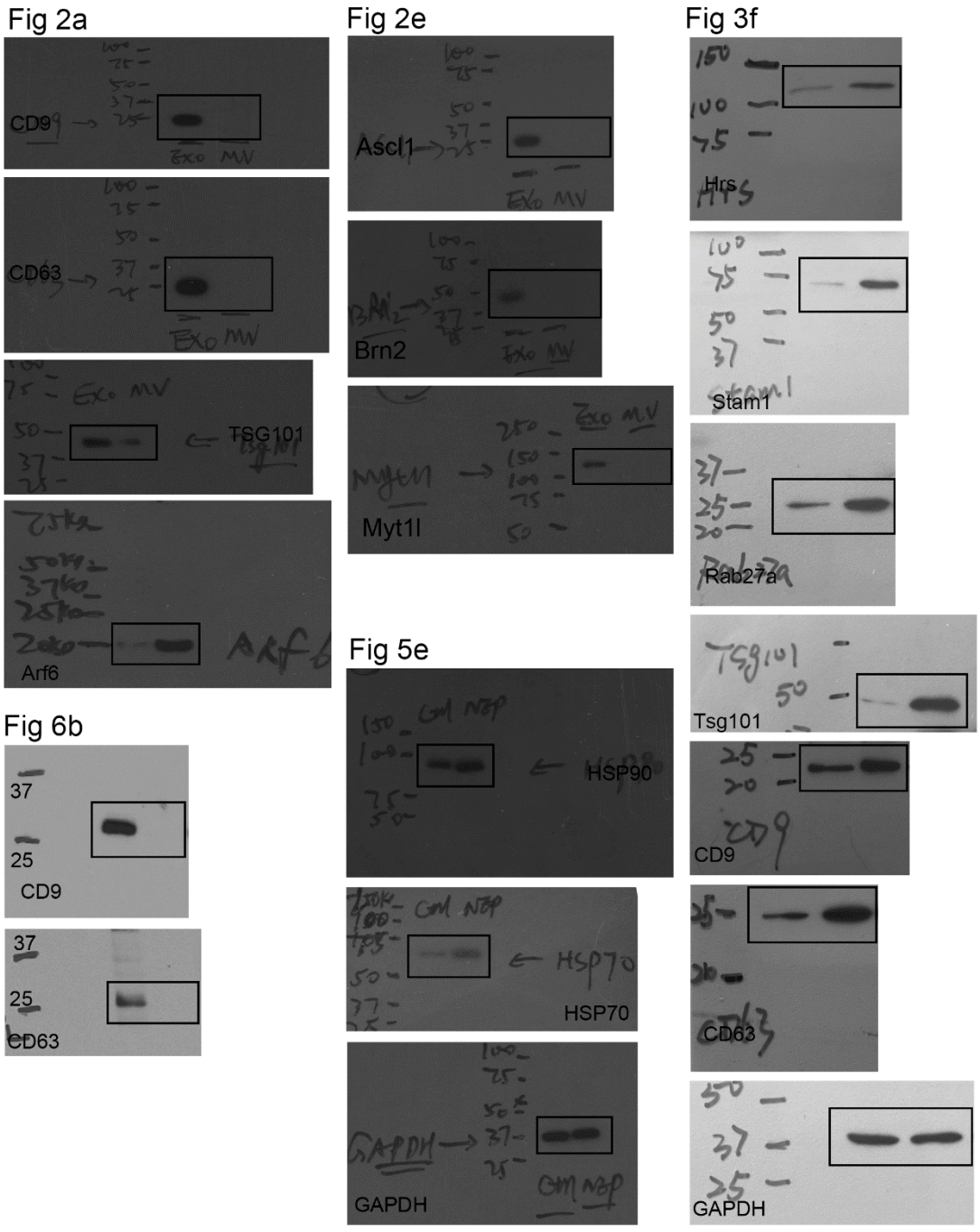

Figure S9. Full scans of the blots in Fig. 2a, 2e, 3f, 5e, and 6b.

Figure S10

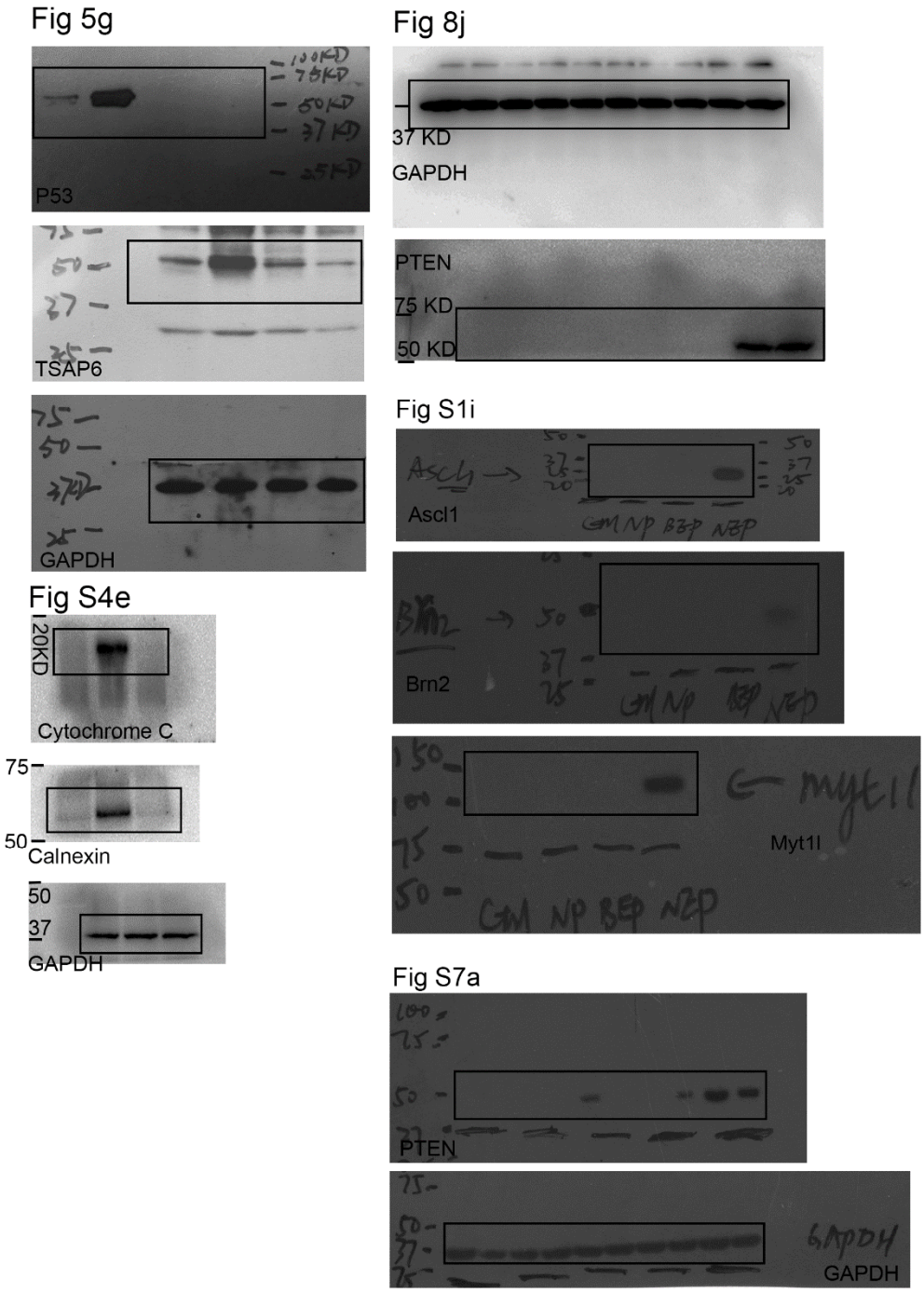

Figure S10. Full scans of the blots in Fig. 5g, 8j, S1i, S4e, and S7a.

Supplementary Video 1 Massive MVB formation 4 h after CNP treatment when CD63-GFP plasmid was delivered by CNP,

Supplementary Video 2 BEP-transfected MEFs only exhibit weak green fluorescence.

Supplementary Video 3 CD63-GFP release after CNP (3x slow motion).

Supplementary Video 4 Fluorescent signal of propidium iodide (PI) dye diffusion via anchored MEF cell membrane pores in CNP. PI diffusion through “top” bulk buffer after CNP.

Supplementary Video 5 PI diffusion in BEP.

Supplementary Video 6 PI diffusion through “bottom” nanochannels.

Supplementary Video 7 Temperature rise by joule heating during CNP treatment as measured with a temperature-sensitive fluorescent dye, Rhodamine B.